BOOK IN STOCK

Recent contributions of remote sensing to the study of internal waves in the straits of Gibraltar and Messina

by

Werner ALPERS, Peter BRANDT, Angelo RUBINO and Jan O. BACKHAUS

Institute of Oceanography, University of Hamburg, Hamburg, Germany.

ABSTRACT

Radar images acquired from 1991 to 1995 by the synthetic aperture radar (SAR) aboard the European Remote Sensing satellites ERS-1 and ERS-2 have been used to study the dynamics of internal solitary waves in the straits of Gibraltar and Messina. Internal waves become visible on radar images because they are associated with a variable surface current which modulates the sea surface roughness and thus the backscattered radar power. Roughness patterns of internal waves which are imaged by the SARs aboard these satellites are compared with surface convergence patterns calculated by recently developed numerical models describing the generation and propagation of internal waves in these straits.

RÉSUMÉ

Grâce aux images radar acquises de 1991 à 1995 par le radar à synthèse d'ouverture (SAR) embarqué à bord des satellites européens ERS-1 et ERS-2, nous avons pu étudier la dynamique des vagues solitaires internes dans les détroits de Gibraltar et de Messine. Les vagues internes deviennent visibles sur les images radar parce qu'elles sont associées à un courant de surface variable qui module la rugosité de la surface de la mer et, par là, l'écho du radar. Nous comparons les modèles des mouvements des vagues internes telles qu'elles sont mises en images par SAR à bord de ces satellites avec les convergences de surface calculées à partir des modèles numériques récemment développés qui décrivent la naissance et la propagation des vagues internes dans ces détroits.

BOOK IN STOCK

INTRODUCTION

Traditionally, oceanic internal wave fields have been measured by instruments deployed in the ocean, like temperature and salinity sensors or current meters, or by acoustic instruments like sonars. However, information on internal wave fields can also be extracted from their sea surface manifestations. For a long time, sailors have reported that periodic bands of increased and reduced roughness are sometimes visible on the ocean surface in certain parts of the world's ocean, in particular in straits and near continental shelves. These roughness bands are often sea surface manifestations of internal waves (OSBORNE and BURCH, 1980). They can be captured by a variety of remote sensing instruments, *e.g.*, by ship radar (CAVANIÉ, 1972, 1973), by photographic cameras flown on air- or spacecrafts (LA VIOLETTE and ARNONE, 1988), by optical scanners flown on satellites (APEL *et al.*, 1975), by ground-based radar (WATSON and ROBINSON, 1990, 1991), or by airborne and spaceborne imaging radars (FU and HOLT, 1983; ALPERS and SALUSTI, 1983; GASPAROVIC *et al.*, 1986; ALPERS and LA VIOLETTE, 1993; RICHEZ, 1994; BRANDT *et al.*, 1996a, 1996b). However, in the past, sea surface manifestations of internal waves have been used only sporadically in systematic studies on internal wave dynamics, *e.g.*, by WATSON and ROBINSON (1990) who monitored the passage of internal waves from the rock of Gibraltar by a shore based radar, and by RICHEZ (1994) who tracked internal wave trains through the Strait of Gibraltar by an airborne synthetic aperture radar (SAR).

In this paper we discuss recent results on the generation and propagation of internal waves in the straits of Gibraltar and Messina based on synthetic aperture radar images acquired by the European Remote Sensing satellites ERS-1 and ERS-2 which were launched on July 17, 1991, and on April 21, 1995, respectively. The identical SARs aboard these satellites operate at a radar frequency of 5.3 GHz, transmit and receive at vertical polarization and illuminate the sea surface at a mean incidence angle of 23 degrees. These SAR images have a nominal resolution of 25 m x 25 m. For our investigation we had available 281 ERS-1/2 SAR scenes from 152 satellite overflights over the Strait of Gibraltar and 266 SAR scenes from 127 overflights over the Strait of Messina.

INTERNAL WAVES IN THE STRAIT OF GIBRALTAR

It is well known that strong internal waves are generated in the Strait of Gibraltar by the interaction of a tidal flow with topographic features (FRASSETTO, 1960, 1964; ZIEGENBEIN, 1969, 1970; CAVANIÉ, 1972, 1973; LACOMBE and RICHEZ, 1982; KINDER, 1984; ARMI and FARMER, 1985, 1988; LA VIOLETTE and LACOMBE 1988; LA VIOLETTE and ARNONE, 1988; PIERINI, 1989; BRAY, 1990; HIBIYA, 1990; PETTIGREW and HYDE, 1990; LONGO *et al.*, 1992; WATSON and ROBINSON, 1990; WANG, 1993; RICHEZ, 1994). The water body in the Strait of Gibraltar and its approaches consists of a deep layer of salty Mediterranean water (salinity approximately 38 psu) and an upper layer of less salty Atlantic water (salinity approximately 36 psu). The mean flow is composed of two counter-flowing layers: an upper layer of Atlantic water flowing into the Mediterranean Sea and a lower layer of Mediterranean water flowing into the Atlantic Ocean. The

BOOK IN STOCK

mean depth of the interface between these two layers slopes down from about 80 m on the Mediterranean side of the strait to about 800 m on the Atlantic side. The relative change of water density across this interface, mainly determined by the salinity difference and therefore called halocline, is 0.002. For a comprehensive summary of the oceanography of the Strait of Gibraltar the reader is referred to the paper of LACOMBE and RICHEZ (1985). The Strait of Gibraltar has a complex bottom topography containing several ridges as depicted in the topographic map shown in Fig. 1. The shallowest section in the Strait of Gibraltar is at the Camarinal Sill where the maximum

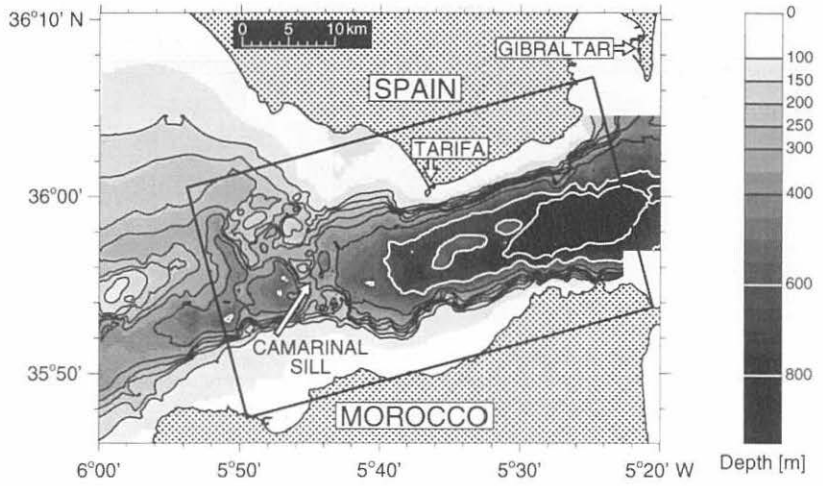


Fig. 1 – Topographic map of the Strait of Gibraltar. The gray shadings indicate the basin depth. The rectangle denotes the area of the ERS-1 SAR images shown in Fig. 5.

water depth is 290 m. The interaction of the predominantly semidiurnal tidal flow with the sills inside the strait, in particular with the Camarinal Sill, gives rise to periodic deformations of the halocline in the sill regions which then give birth to internal solitary waves. Fig. 2 shows a typical ERS-1 SAR image which was acquired on Jan. 20, 1994, at 1103 UTC (orbit: 13151, frames: 2871/2889). It shows sea surface manifestations of an internal bore inside the Strait of Gibraltar (single curved bright line in the center of the image) and of an internal wave train propagating into the Mediterranean Sea (right hand section of the image). It can be inferred from the distance between both features that the internal wave train was generated one tidal cycle before the internal bore was generated.

A numerical oceanic model which describes the generation and propagation of internal waves in the Strait of Gibraltar has recently been developed by BRANDT *et al.* (1996a). In this model the hydrodynamic equations are approximated by nonlinear, weakly nonhydrostatic, shallow water equations for a two layer ocean. It depends on one space variable only, but it retains several features of a fully three-dimensional model by including a realistic bottom topography and a variable channel width. Fig. 3 shows the

BOOK IN STOCK

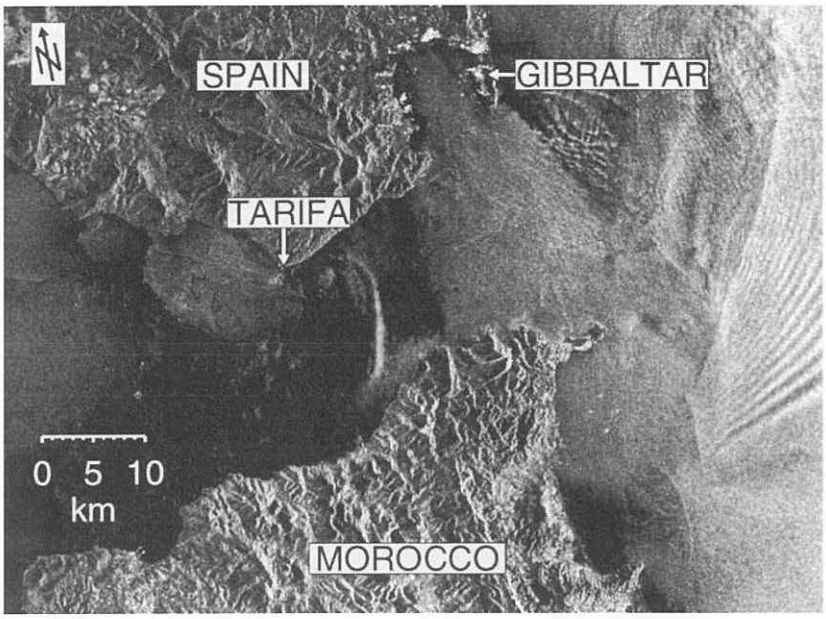


Fig. 2 – ERS-1 SAR image of the Strait of Gibraltar acquired on Jan. 20, 1994, at 1103 UTC, 9 h 17 min after low tide at Tarifa. It shows sea surface manifestations of an internal bore inside the strait (single curved bright line in the center) and an internal wave train east of the strait (right hand section of the image) which was generated one tidal cycle before the internal bore was generated.

form of the interface at four different times of the tidal cycle as calculated by this model. The light gray shaded areas mark the regions where the flow is supercritical, *i.e.*, where the internal Froude number G is larger than one. For $G > 1$, the phase speed of internal waves is smaller than the current velocity. Internal disturbances which propagate against the flow are trapped in the transition region between subcritical ($G < 1$) and supercritical flow ($G > 1$). The transition between these two flow regimes (subcritical and supercritical) is called internal hydraulic jump. For a detailed discussion on this issue the reader is referred to the papers of ARMI and FARMER (1985, 1988) and GARRETT (this volume). During strong westward tidal flow, internal hydraulic jumps occur downstream of the Camarinal Sill, the Spartel Sill and the sub-ridges located 7 km west and 4 km east of the Camarinal Sill (Fig. 3a). At this time, the tidal flow is in the same direction as the mean flow in the lower layer, and an interfacial uplift at the Camarinal Sill develops which is followed by a strong interfacial depression at the downstream side of the sill. When the westward tidal flow slackens (Fig. 3b), this interfacial depression, also called internal bore, is released from the Camarinal Sill and propagates eastwards. On propagating eastwards, the bore steepens and finally decays into a train of internal solitary waves (Fig. 3c). With the reversal of the tidal flow direction, the internal bore enters the Tarifa Narrows and is advected eastwards by the strong flow in the upper layer. During maximum eastward tidal flow (Fig. 3c), there exists a small region

BOOK IN STOCK

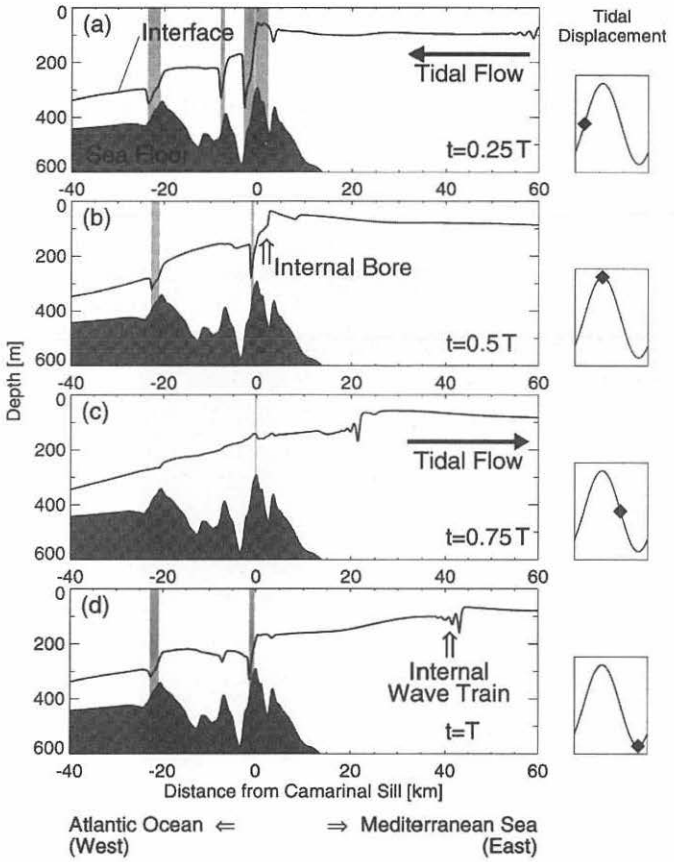


Fig. 3 – Form of the halocline (interface between the two layers) at different phases of the tidal cycle as a function of distance from the Camarinal Sill (x=0) as calculated by the numerical model of BRANDT *et al.* (1996a). The time t=0 corresponds to low tide. The light gray shaded areas mark the regions where the flow is supercritical. These plots illustrate how the form of the interface varies during one tidal cycle (T is the tidal period) and how a train of internal solitary waves evolves from an internal bore.

at the Camarinal Sill where the supercritical flow, which lasts there for about one hour, leads to the generation of a very weak westward propagating internal bore. This asymmetry in the strength of internal hydraulic jumps at the Camarinal Sill is a consequence of the fact that the mean flow in the lower layer is directed towards the Atlantic Ocean. This leads to the observed east-west asymmetry of the internal wave field: westward propagating internal waves linked to the halocline are much weaker than eastward propagating ones (see also HIBIYA, 1990).

It is well known that internal waves are associated with a variable surface current which modulates the surface roughness and thus the radar backscattering (see for instance ALPERS, 1985; THOMPSON *et al.*, 1988; APEL *et al.*, 1988). To first order, the modulation of the backscattered radar power is pro-

BOOK IN STOCK

portional to the surface convergence (ALPERS, 1985). Thus the calculated surface convergence pattern reflects the image intensity modulation visible in a radar image. Fig. 4 shows how the calculated surface convergence patterns associated with the internal waves vary as a function of space (distance from the Camarinal Sill) and time (time after low tide at Tarifa). This space-time diagram clearly depicts the east-west asymmetry of the internal wave field: only eastward propagating internal waves can be delineated in this diagram. Furthermore, it shows a strong quasi-stationary surface convergence pattern slightly west of the Camarinal Sill. This pattern, which lasts for approximately four hours (centered at about maximum westward tidal flow), is associated with the strong depression of the interface in this region.

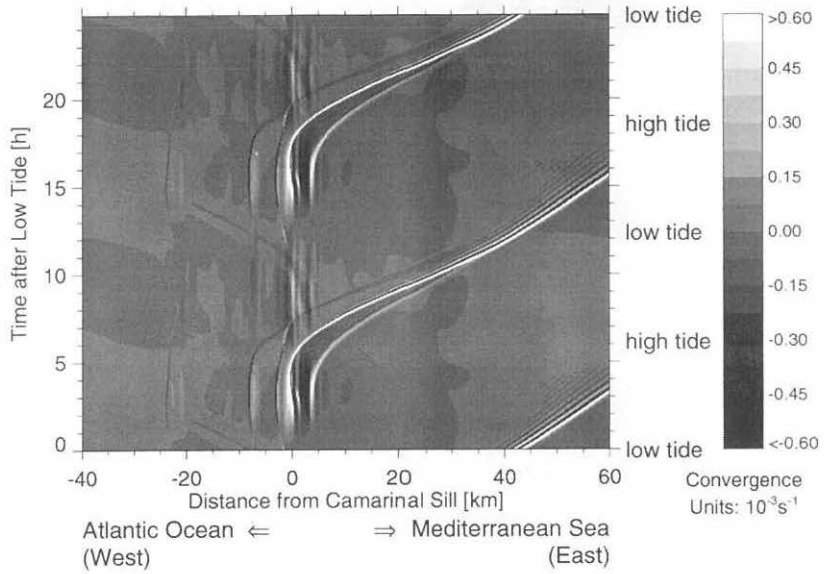


Fig. 4 – Space-time diagram showing the evolution of internal wave disturbances generated at the Camarinal Sill by the action of the tide as a function of distance from the sill (x=0) and time after low tide (t=0) as calculated by the model. The gray shadings indicate the strength of the surface convergence and are, to first order, proportional to the variation of the backscattered radar power.

Fig. 5 shows two examples of SAR images in which roughness patterns at the Camarinal Sill are visible. They can be interpreted as sea surface manifestations of strong depressions of the interface in this region. The upper image (Fig. 5a) was acquired on Jan. 08, 1993, at 1105 UTC (orbit: 7754, frames: 2871/2889), approximately at maximum westward tidal flow (2 h 47 min after low tide at Tarifa). At this time the roughness pattern at the Camarinal Sill was found at its furthest western limit. The lower image (Fig. 5b) was acquired on Jan. 08, 1994, at 1103 UTC (orbit: 12979, frames: 2871/2889), approximately at slack water after westward tidal flow (5 h 31 min after low tide at Tarifa). At this time the roughness pattern was located east of the Camarinal Sill. It can be interpreted as the sea surface manifestation of an internal bore propagating eastwards.

BOOK IN STOCK

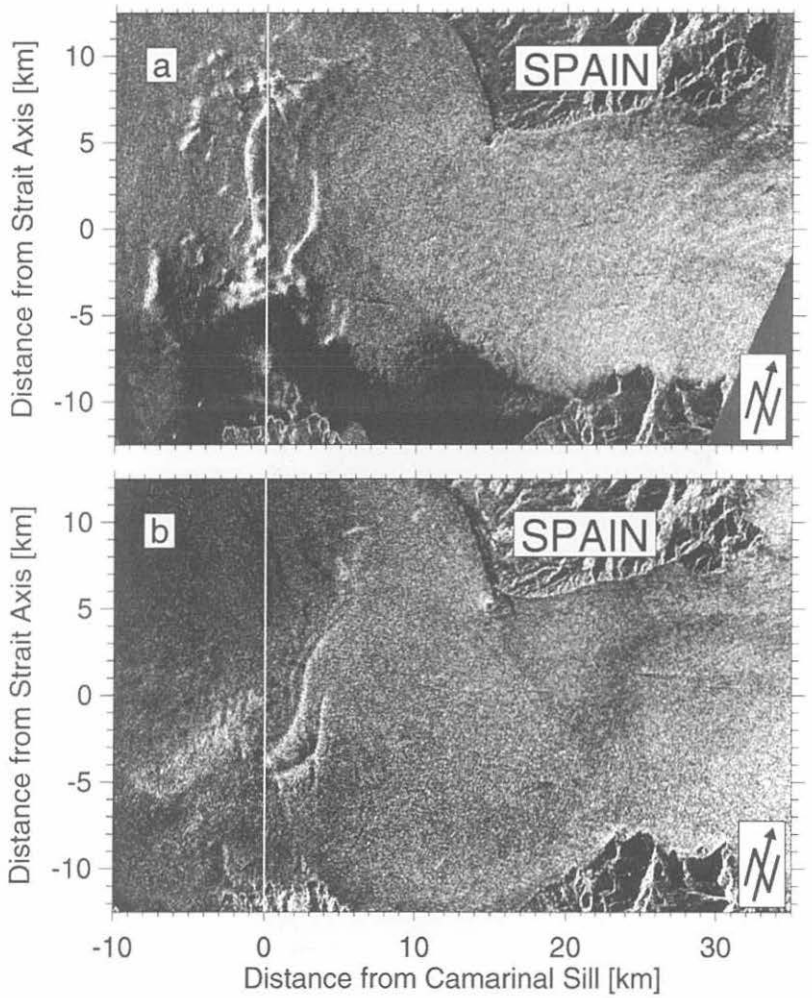


Fig. 5 – Two ERS-1 SAR images of the Strait of Gibraltar including the Camarinal Sill acquired at different phases of the tidal cycle: (a) 2 h 47 min after low tide at Tarifa (Jan. 08, 1993, 1105 UTC); (b) 5 h 31 min after low tide at Tarifa (Jan. 08, 1994, 1103 UTC). The upper image (a) was acquired approximately at maximum westward tidal flow and the lower image (b) approximately at slack water after maximum westward tidal flow. The images show bright lines near the Camarinal Sill which are sea surface manifestations of strong depressions of the halocline.

Fig. 6 shows an ERS-1 SAR image of the Alboran Sea east of the Strait of Gibraltar acquired on Oct. 12, 1994, at 1059 UTC (orbit: 11719, frames: 2871/2889). Sea surface manifestations of two internal wave trains generated at successive tidal cycles can be delineated. The most eastern wave train has a lateral extent of more than 110 km, reaching almost from the Spanish to the Moroccan coast. Since the ERS-1 SAR swath captured only a part of this quasi-spherical wave train, we have extrapolated the pattern eastwards.

BOOK IN STOCK

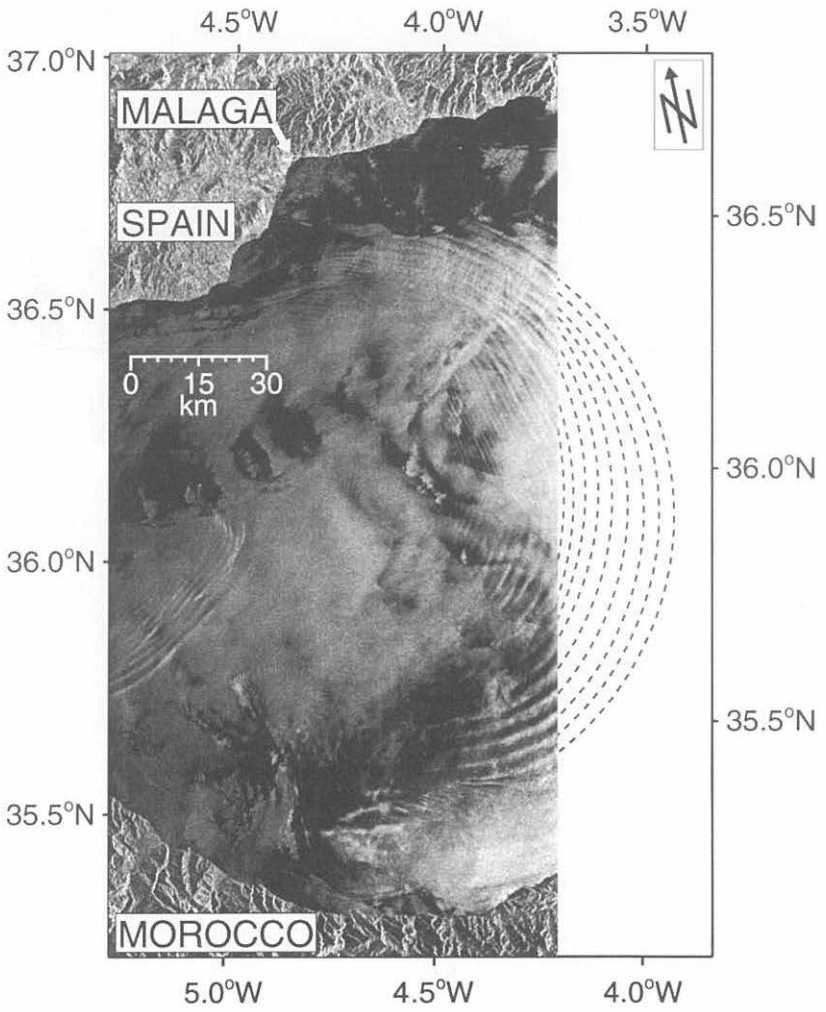


Fig. 6 – ERS-1 SAR image acquired on Oct. 12, 1993, at 1059 UTC over the Alboran Sea (western Mediterranean Sea) south of the Spanish city of Malaga. It shows sea surface manifestations of two internal wave trains generated in the Strait of Gibraltar. The sea surface manifestations associated with the most eastern wave train has been extrapolated outside the image. The distance between the leading edge of this wave train and Gibraltar is approximately 150 km.

Using this extrapolation, we infer that the wave train extends as far as 150 km from the eastern mouth of the Strait of Gibraltar into the Alboran Sea. It seems that this image provides, for the first time, evidence that internal waves generated in the Strait of Gibraltar travel that far east. Furthermore, from the distance between the fronts of the two wave trains and the period of the tidal cycle (12.4 h), we infer that the propagation speed was 2.1 m/s.

Fig. 7 shows an ERS-1 SAR image acquired on Aug. 5, 1994, at 2241 UTC (orbit: 15984, frame:711), on which an internal wave train propagating

BOOK IN STOCK

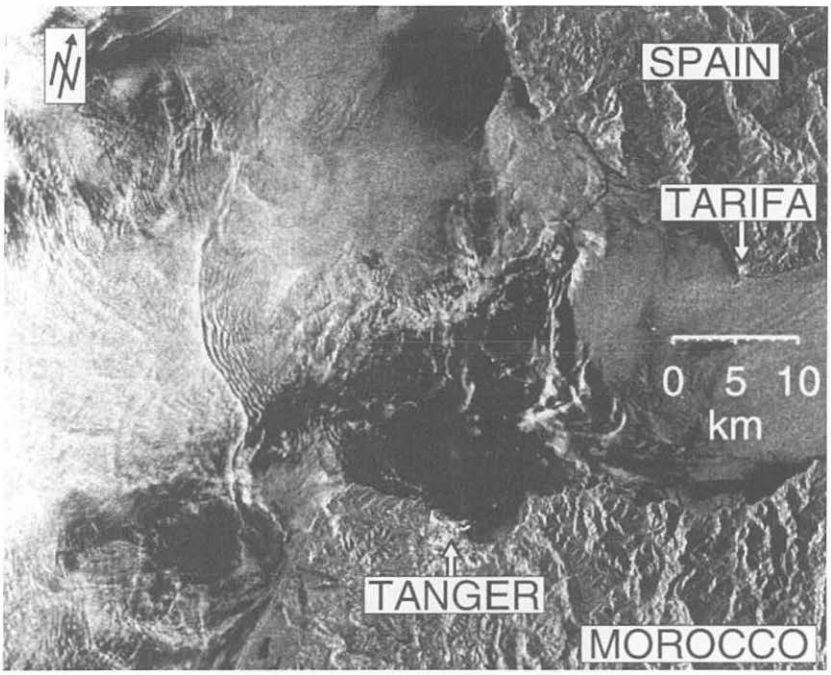


Fig. 7 – ERS-1 SAR image of the Strait of Gibraltar acquired on Aug. 5, 1994, at 2241 UTC, 3 h 8 min after low tide at Tarifa. It shows sea surface manifestations of an internal wave train propagating out of the Strait of Gibraltar towards the Atlantic Ocean. Note the small wavelengths in this wave train as compared to the wavelengths in wave trains propagating into the Mediterranean Sea. Probably, this internal wave train is linked to a seasonal thermocline.

westwards into the Atlantic Ocean can be delineated. As far as we know, this is the first time that such an internal wave train propagating from the Strait of Gibraltar into the Atlantic Ocean has been detected. The short wavelengths suggest that this internal wave train is not linked to the halocline. Probably, it is linked to a seasonal thermocline which forms during summer.

INTERNAL WAVES IN THE STRAIT OF MESSINA

The Strait of Messina is a narrow channel which separates the Italian peninsula from the island of Sicily and connects the Tyrrhenian Sea north of the strait with the Ionian Sea south of it. A topographic map of the Strait of Messina is shown in Fig. 8. The shallowest section in this strait has a cross-section of 0.3 km^2 in the sill region, where the mean water depth is 80 m. While in the southern part of the strait the bottom slopes down very steeply to a depth of more than 800 m approximately 15 km south of the sill, the northern region has a more gentle slope. Here the 400 m isobath is located approximately 15 km north of the sill. Throughout the year, two different water masses are encountered in the Strait of Messina: the Tyrrhenian Surface Water and the colder and saltier Levantine Intermediate Water. In the vicinity of the Strait of Messina these water masses are separated at a depth of approximately 150 m (VERCELLI, 1925). During most of the year, a

BOOK IN STOCK

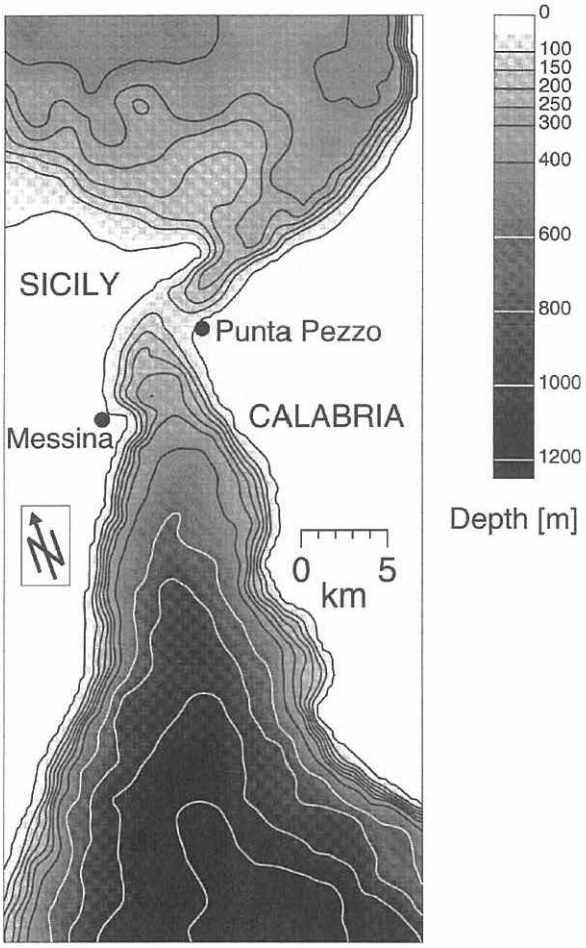


Fig. 8 – Topographic map of the Strait of Messina. The gray shadings indicate the basin depth.

seasonal thermocline is also present in the strait which overlies this weak stratification. Although tidal displacements are very small in the Mediterranean Sea (on order of 10 cm), large gradients of tidal displacements are encountered in the Strait of Messina, because the predominantly semidiurnal tides north and south of the strait are approximately in phase opposition. Due to the phase opposition of the tide and due to topographic constrictions, the current velocities can attain values as high as 3.0 m/s in the sill region (VERCELLI, 1925; DEFANT, 1961).

These hydrological peculiarities of the Strait of Messina may explain why this site has attracted the attention of many ancient writers and philosophers. HOMER (800 B.C.) makes two monsters, Scylla and Charybdis, responsible for the violent currents in the strait (HOMER, *Odyssey,* 12th song, line 80-114). ARISTOTLE (384-322 B.C.) argues that hollows in the sea floor

BOOK IN STOCK

and the interaction of two opposing wind-generated currents produce such intensive currents (ARISTOTLE, *Problema Physica*, chap. 23) and, in the poetry of ancient times, allegories alluding to the tremendous danger of sailing in the Strait of Messina can often be found ("*Incidis in Scyllam cupiens vitare Charybdim*", APOSTOLIUS). But more than 2000 years elapsed before scientific oceanographic measurements were carried out in this area. In 1922, during two cruises with the research vessel *Marsigli*, the Italian oceanographer VERCELLI made the first extensive oceanographic survey of this area. The oceanographic data collected by VERCELLI are still considered to be the most detailed and systematic data of the Strait of Messina until now (VERCELLI, 1925; VERCELLI and PICOTTI, 1925). However, these mesurements did not focus on tidally generated internal waves. The first observation of internal waves generated in the Strait of Messina was made by the synthetic aperture radar (SAR) aboard the American Seasat satellite on Sept. 15, 1978. The three rings visible on the Seasat SAR image of the Tyrrhenian Sea north of the strait were interpreted as sea surface manifestations of a train of internal solitary waves propagating northwards (ALPERS and SALUSTI, 1983). In the following years internal waves propagating north- as well as southwards have been detected during several oceanographic campaigns (ALPERS and SALUSTI, 1983; GRIFFA *et al.*, 1986; DI SARRA *et al.*, 1987; SAPIA and SALUSTI, 1987; NICOLÓ and SALUSTI, 1991). The first observation of a well developed internal wave train south of the sill was made on June 20, 1984, by the thematic mapper (TM) aboard the Landsat-5 satellite (ARTALE *et al.*, 1990). In October 1987 NICOLÓ and SALUSTI (1990) also measured large amplitude internal waves by a temperature sensor deployed in the ocean south of the sill. A review of recent oceanographic investigations carried out in the Strait of Messina up to 1990 can be found in BIGNAMI and SALUSTI (1990).

Since 1991, a large number of ERS-1/2 SAR images have been acquired over the Strait of Messina. They often show sea surface manifestations of northward and southward propagating internal waves. Fig. 9 shows an ERS-1 SAR image which was acquired on Aug. 17, 1995, at 2113 UTC (orbit: 21388, frames: 747/765). On this image sea surface manifestations of three internal wave trains propagating southwards and one propagating northwards can be delineated.

A numerical oceanic model which describes the generation and propagation of internal waves in the Strait of Messina has recently been developed by BRANDT *et al.* (1996b) which is similar to the model developed previously for the Strait of Gibraltar (BRANDT *et al.*, 1996a). Fig. 10 shows the form of the interface at six different times of the tidal cycle as calculated by this model. At the bottom of this figure the depth profile used in the numerical simulations is shown. The light gray shaded areas mark the regions where the flow is supercritical. We have carried out the simulations with an undisturbed interface depth of 30 m and a relative density difference between the two water layers of 0.0015. These parameters are typical for a well developed seasonal thermocline. In contrast to the Strait of Gibraltar, no significant mean exchange flow exists in the Strait of Messina. Thus, during northward tidal flow (Fig. 10a), an interfacial depression develops north and, during southward tidal flow (Fig. 10d), an interfacial depression develops south of the sill. When the tidal flow slackens, internal bores are

BOOK IN STOCK

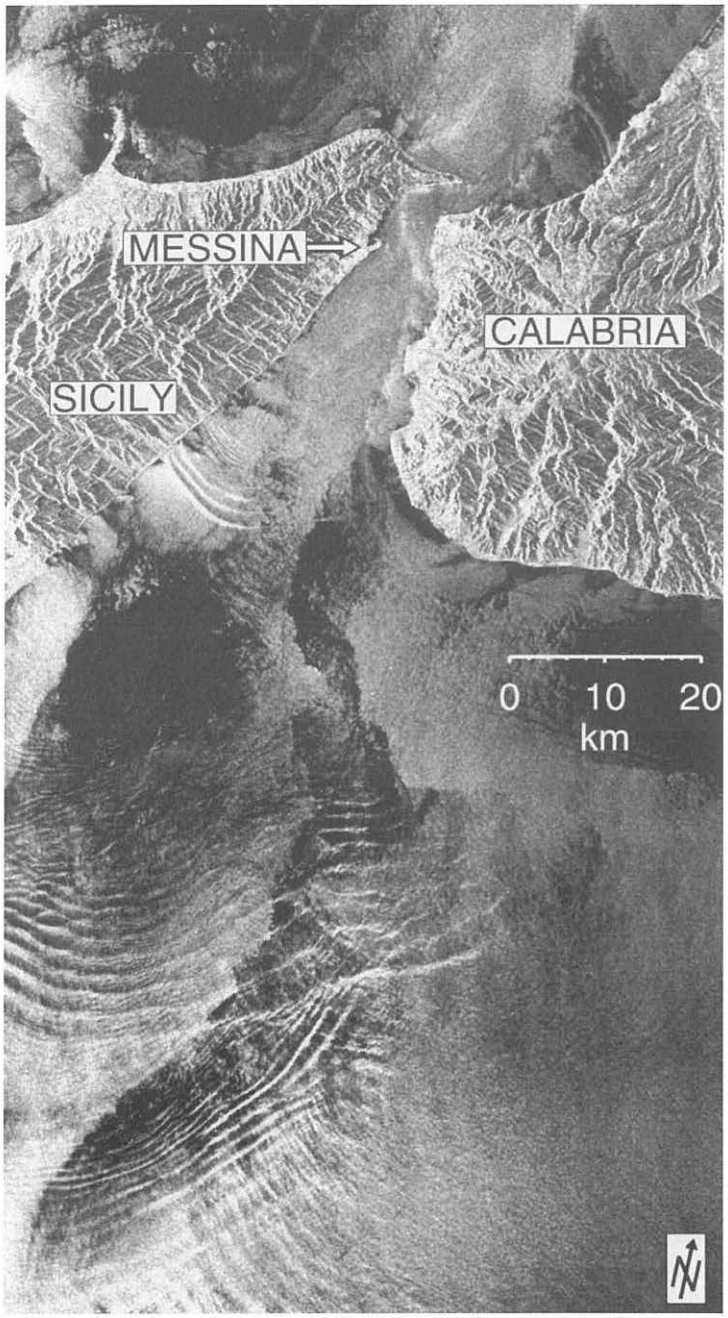


Fig. 9 – ERS-1 SAR image of the Strait of Messina acquired on Aug. 17, 1995, at 2113 UTC, 12 h 26 min after maximum northward tidal flow at Punta Pezzo. It shows sea surface manifestations of three internal wave trains propagating southwards and one propagating northwards.

BOOK IN STOCK

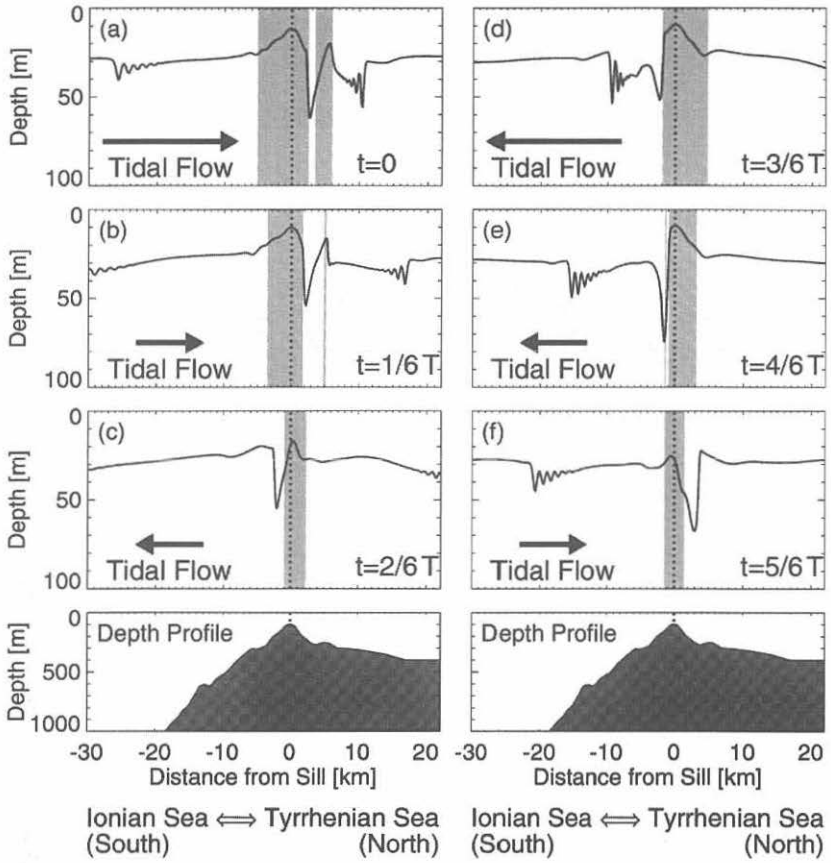


Fig. 10 – Form of the interface between the two layers at different phases of the tidal cycle as a function of distance from the sill (x=0) as calculated by the numerical model of BRANDT *et al.* (1996b). The time t=0 coresponds to maximum northward tidal flow. The light gray shaded areas mark the regions where the flow is supercritical. These plots illustrate how the form of the interface varies during one tidal cycle (T is the tidal period) and how a train of internal solitary waves evolves. In the bottom panels the depth profile is depicted. The vertical dotted lines mark the position of the sill.

released from the sill, which propagate in the first case southwards and in the second case northwards. These internal bores then decay into trains of internal solitary waves. However, due to the different topography north and south of the sill, northward propagating internal solitary waves have, in general, smaller amplitudes than southward propagating ones (see Fig. 10b and 10e). Fig. 11 shows a space-time diagram delineating the evolution of the surface convergence patterns associated with internal waves as calculated by the model. Noticeable is the long persistence of the surface convergence patterns associated with interfacial depressions north and south of the sill during northward as well as during southward tidal flow, respectively. Several model runs, performed with different values for the density difference between the two water layers and for the depths of the undisturbed

BOOK IN STOCK

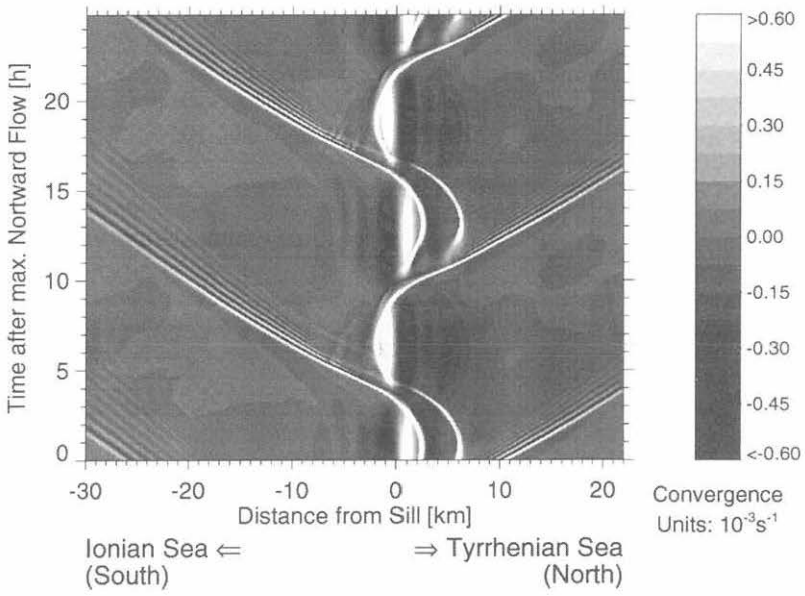


Fig. 11 – Space-time diagram showing the evolution of internal wave disturbances generated at the sill in the Strait of Messina by the action of the tide as a function of distance from the sill (x=0) and time after maximum northward tidal flow (t=0) as calculated by the model. The gray levels indicate the strength of the surface convergence and are, to first order, proportional to the variation of the backscattered radar power.

interface, indicate that the observed internal wave field is linked to the seasonal thermocline rather than to the permanent stratification caused by the presence of Tyrrhenian Surface Water and Levantine Intermediate Water in the Strait of Messina. A statistical analysis of the available ERS-1/2 SAR images confirms these model results. In fact, the ERS-1/2 SAR images show that sea surface manifestations of internal waves are observed more frequently during periods where a strong seasonal thermocline is known to be present. Furthermore, we have noticed that sea surface manifestations of southward propagating internal wave trains are more often visible on ERS-1/2 SAR images than those of northward propagating internal wave trains. The SAR image depicted in Fig. 9 shows evidence of such a north-south asymmetry. In general, sea surface manifestations of southward propagating internal waves are stronger than those of northward propagating ones. Often the internal wave trains have a very regular form as evident from the ERS-1 SAR image acquired on Oct. 26, 1995, at 2113 UTC (orbit: 22390, frames: 747/765) which is depicted in Fig. 12. This image, as well as the one shown in Fig. 9, delineates that the sea surface manifestations of the southward propagating internal waves are stronger near the Sicilian coast than further offshore. Thus the amplitude of the internal waves must be larger in this shallow water region, where the internal waves are topographically guided.

Figs. 13 and 14 show two ERS-1 SAR images acquired on July 11, 1993, at 0941 UTC (orbit: 10387, frame: 2835) and on July 13, 1995, at

BOOK IN STOCK

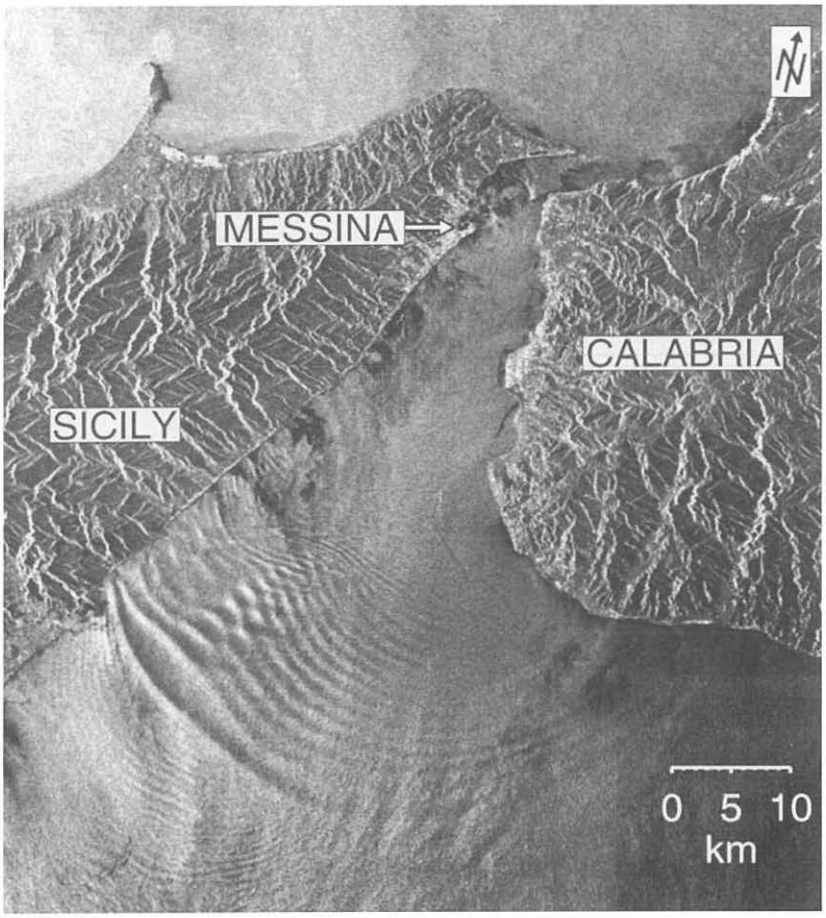


Fig. 12 – ERS-1 SAR image of the Strait of Messina acquired on Oct. 26, 1995, at 2113 UTC, 3 h 25 min after maximum northward tidal flow at Punta Pezzo. It shows sea surface manifestations of a very regular wave train consisting of more than 16 waves propagating southwards. Note that the sea surface manifestations are stronger near the Sicilian coast than further offshore.

2114 UTC (orbit: 20887, frame: 765). On both images sea surface manifestations of northward propagating internal solitary waves are visible. Note the pronounced differences in form, wavelength and modulation depth of the sea surface manifestations of these two wave trains. The internal wave train visible on the image depicted in Fig. 13 has a strong surface signature and a weak wave front curvature. It propagates along the Calabrian coast in the direction of the strait axis. On the contrary, the internal wave train visible on the image depicted in Fig. 14 has a weak surface signature. It propagates almost spherically from the northern mouth of the Strait of Messina into the Tyrrhenian Sea. The large variability in the sea surface manifestations of northward propagating internal waves is a general feature which we have noticed in the analysis of the ERS-1/2 SAR images. At present, we have no explanation for this observed variability.

BOOK IN STOCK

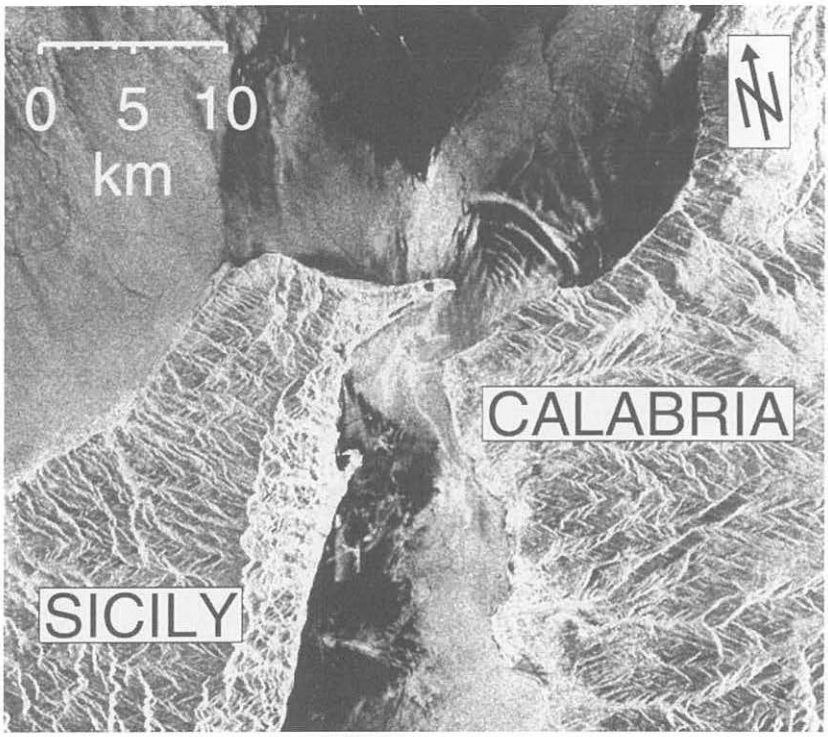


Fig. 13 – ERS-1 SAR image of the Strait of Messina acquired on July 11, 1993, at 0941 UTC, 20 min after maximum northward tidal flow at Punta Pezzo. It shows sea surface manifestations of a northward propagating internal wave train.

CONCLUSIONS

The analysis of synthetic aperture radar images from the European Remote Sensing satellites ERS-1 and ERS-2 acquired over the straits of Gibraltar and Messina has significantly contributed to the understanding of the internal wave dynamics in these straits. For the first time, internal waves radiating from the Strait of Gibraltar into the Mediterranean Sea have been detected as far as 150 km east of Gibraltar. Furthermore, an internal wave train propagating westward from the Strait of Gibraltar into the Atlantic Ocean has been detected on one ERS-1 SAR image. However, this wave train is very likely not linked to the halocline, but rather to a seasonal thermocline present in this region during summer.

In the Strait of Messina, both southward and northward propagating internal waves are observed, but southward propagating internal waves are more frequent than northward propagating ones. In general, southward propagating waves are stronger than northward propagating ones and they are topographically guided along the Sicilian coast. Internal waves propagating northwards into the Tyrrhenian Sea exhibit a large variability, whose cause is not understood yet.

BOOK IN STOCK

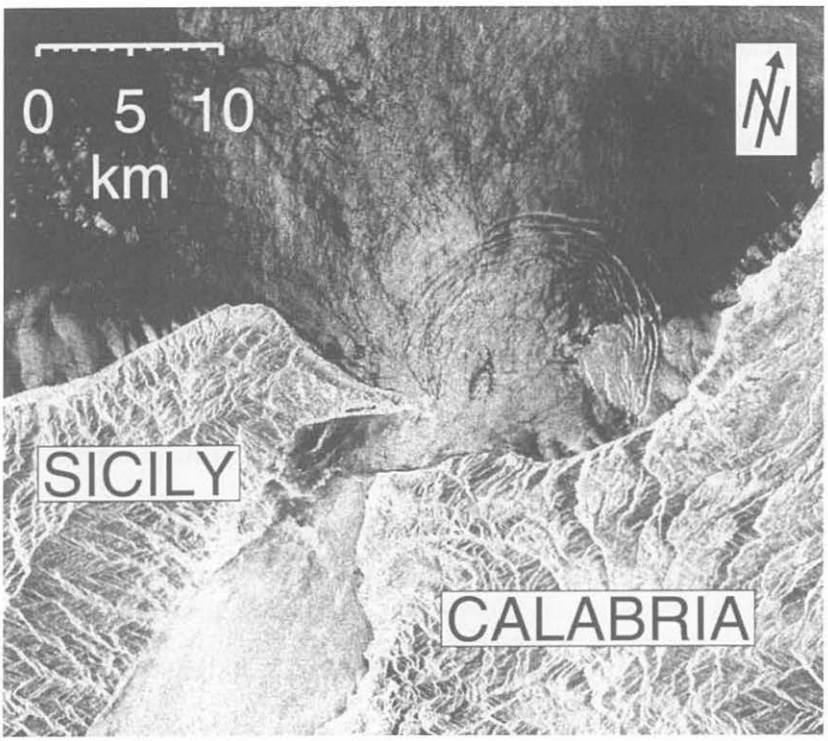


Fig. 14 – ERS-1 SAR image of the Strait of Messina acquired on July 13, 1995, at 2114 UTC, 3 h 57 min after maximum northward tidal flow at Punta Pezzo. It shows sea surface manifestations of a northward propagating internal wave train.

ACKNOWLEDGMENTS

We thank the European Space Agency (ESA) for supplying the ERS-1/2 SAR images and F. Roca from SECEG, Madrid (Spain) for providing the digital topographic map of the Strait of Gibraltar. This work has been supported by the German Space Agency (DARA), under contract 50 EE 9413.

REFERENCES

ALPERS W., 1985. — Theory of radar imaging of internal waves. — *Nature,* **314**: 245-247.

ALPERS W., SALUSTI E., 1983. — Scylla and Charybdis observed from space. — *J. Geophys. Res.*, **88**: 1800-1808.

ALPERS W., LA VIOLETTE P.E., 1993. — Tide-generated nonlinear internal wave packets in the Strait of Gibraltar observed by the synthetic aperture radar aboard the ERS-1 satellite. — Proceedings of the First ERS-1

BOOK IN STOCK

Symposium, held in Cannes, France, Nov. 4-6, 1992, published by ESA Publications Division, ESTEC, Noordwijk, The Netherlands, ESA SP-**359, 2**: 753-758.

APEL J.R., BYRNE H.M., PRONI J.R., CHARNELL R.L., 1975. — Observation of oceanic internal waves from the Earth Resources Technology Satellite. — *J. Geophys. Res.*, **80**: 865-881.

APEL J.R., GASPAROVIC R.F., THOMPSON D.R., GOTWOLS B.L., 1988. — Signatures of surface/internal wave interactions: Experiment and theory. — *Dynam. Atmos. Oceans*, **12**: 89-106.

ARMI L., FARMER D., 1985. — The internal hydraulics of the Strait of Gibraltar and associated sills and narrows. — *Oceanol. Acta,* **8**: 37-46.

ARMI L., FARMER D., 1988. — The flow of Mediterranean water through the Strait of Gibraltar. — *Prog. Oceanogr.*, **21**: 1-105.

ARTALE V., LEVI D., MARULLO S., SANTOLIERI R., 1990. — Analysis of nonlinear internal waves observed by Landsat thematic mapper. — *J. Geophys. Res.*, **95**: 16065-16073.

BIGNAMI F., SALUSTI E., 1990. — Tidal currents and transient phenomena in the Strait of Messina: a review. — *In*: Pratt, L.J. ed., The Physical Oceanography of Sea Straits., Kluwer Academic, Boston, p. 95-124.

BRAY N.A., WINANT C.D., KINDER T.H., CANDELA J., 1990. — Generation and kinematics of the internal tide in the Strait of Gibraltar. — *In*: Pratt, L.J. ed., The Physical Oceanography of Sea Straits., Kluwer Academic, Boston, p. 477-491.

BRANDT P., ALPERS W., BACKHAUS J.O., 1996a. — Study of the generation and propagation of internal waves in the Strait of Gibraltar using a numerical model and synthetic aperture radar images from the European ERS-1 satellite. — *J. Geophys. Res.*, in press.

BRANDT P., RUBINO A., ALPERS W., BACKHAUS J.O., 1996b. — Internal waves in the Strait of Messina studied by a numerical model and synthetic aperture radar images from the European ERS-1 satellite. — submitted to *J. Phys. Oceanogr.*

CAVANIÉ A.G., 1972. — Observations de fronts internes dans le détroit de Gibraltar pendant la campagne océanographique OTAN, 1970, et interprétation des résultats par un modèle mathématique. — *Mem. Soc. Roy. Sci.*, Liège, **6**(II): 27-41.

CAVANIÉ A.G., 1973. — Observations océanographiques dans le détroit de Gibraltar pendant la campagne PHYGIB (Sept-Oct 1971). — *Annales Hydrographiques*, **1**: 75-84.

DEFANT A., 1961. Physical Oceanography, 2 volumes, Pergamon, New York.

DI SARRA A., PACE A., SALUSTI E., 1987. — Long internal waves and columnar disturbances in the Strait of Messina. — *J. Geophys. Res.*, **92**: 6495-6500.

FARMER D., ARMI L., 1988. — The flow of Atlantic water through the Strait of Gibraltar. — *Prog. Oceanogr.*, **21**: 1-105.

BOOK IN STOCK

FRASSETTO R., 1960. — A preliminary survey of thermal microstructure in the Strait of Gibraltar. — *Deep-Sea Res.*, **7**: 152-162.

FRASSETTO R., 1964. — Short period vertical displacements of the upper layer in the Strait of Gibraltar. — Tech. Rep., 30, SACLANT ASW Res. Centre, La Spezia, Italy, 49 p.

FU L.L., HOLT B., 1984. — Internal waves in the Gulf of California: Observations from a spaceborne radar. — *J. Geophys. Res.*, **89**: 2053-2060.

GARRETT C., 1996. — The role of the Strait of Gibraltar in the evolution of Mediterranean water, properties and circulation. — *In*: Dynamics of mediterranean straits and channels., Briand F. ed., CIESM Science Series n°2, *Bulletin de l'Institut océanographique, Monaco,* n° spécial **17**:1-19

ASPAROVIC R.F., APEL J.R., THOMPSON D.R., TOCHKO J.S., 1986. — A comparison of SIR-B synthetic aperture radar data with ocean internal wave measurements. — *Science,* **232**: 1529-1531.

GRIFFA A., MARULLO S., SANTOLIERI R., VIOLA A., 1986. — Preliminary observations of large-amplitude tidal internal waves near the Strait of Messina. — *Cont. Shelf Res.*, **6**: 677-687.

HIBIYA T., 1990. — Generation mechanism of internal waves by a vertically sheared tidal flow over a sill.— *J. Geophys. Res.*, **95**: 1757-1764.

KINDER T.H., 1984. — Net mass transport by internal waves near the Strait of Gibraltar. — *Geophys. Res. Letters*, **11**: 987-990.

LACOMBE H., RICHEZ C., 1982. — The regime of the Strait of Gibraltar. — *In*: NIHOUL J.C.J. ed., Hydrodynamics of Semi-Enclosed Seas., Elsevier, Amsterdam, p. 13-73.

LA VIOLETTE P.E., LACOMBE H., 1988. — Tidal-induced pulses in the flow through the Strait of Gibraltar. — *Oceanol. Acta*, SP **9**: 13-27.

LA VIOLETTE P.E., ARNONE R.A., 1988. — A tide-generated internal waveform in the western approaches to the Strait of Gibraltar. — *J. Geophys. Res.*, **93**: 15653-15667.

LONGO A.M., MANZO M., PIERINI S., 1992.— A model for the generation of nonlinear internal tides in the Strait of Gibraltar.— *Oceanol. Acta*, **15**: 233-243.

NICOLÓ L., SALUSTI E., 1991. — Field and satellite observations of large amplitude internal tidal wave trains south of the Strait of Messina, Mediterranean Sea. — *Ann. Geophys.*, **9**: 534-539.

OSBORNE A.R., BURCH T.I., 1980. — Internal solitons in the Andaman Sea. — *Science,* **208**: 451-460.

PETTIGREW N.R., HYDE R.A., 1990. — The structure of the internal bore in the Strait of Gibraltar and its influence on the Atlantic inflow. — *In*: Pratt, L.J. ed.; The Physical Oceanography of Sea Straits, Kluwer Academic, Boston, p. 493-508.

PIERINI S., 1989. — A model for the Alboran Sea internal solitary waves. — *J. Phys. Oceanogr.*, **19**: 755-772.

RICHEZ C., 1994. — Airborne synthetic aperture radar tracking of internal waves in the Strait of Gibraltar. — *Prog. Oceanogr.*, **33**: 93-159.

BOOK IN STOCK

SAPIA A., SALUSTI E., 1987. — Observation of non-linear internal solitary wave trains at the northern and southern mouths of the Strait of Messina. — *Deep-Sea Res.*, **34**: 1081-1092.

THOMPSON D.R., GOTWOLS B.L., STERNER R.E., 1988. — A comparison of measured surface wave spectral modulation with predictions from a wave-current interaction model. — *J. Geophys. Res.*, **93**: 12339-12380.

VERCELLI F., 1925. — Il regime dello correnti e delle maree nello stretto di Messina. — Comm. Int. del Mediterraneo, Venice, Italy.

VERCELLI F., PICOTTI M., 1925. — Il regimo fisico-chimico delle acque nello stretto di Messina. — Comm. Int. del Mediterraneo, Venice, Italy.

WANG D.P., 1993. — The Strait of Gibraltar model: internal tide, diurnal inequality and fortnightly modulation. — *Deep-Sea Res.*, **40**: 1187-1203.

WATSON G., ROBINSON I.S., 1990. — A study of internal wave propagation in the Strait of Gibraltar using shore-based marine radar images. — *J. Phys. Oceanogr.*, **20**: 374-395.

ZIEGENBEIN J., 1969. — Short internal waves in the Strait of Gibraltar. — *Deep Sea Res.*, **16**: 479-487.

ZIEGENBEIN J., 1970. — Spatial observations of short internal waves in the Strait of Gibraltar. — *Deep-Sea Res.*, **17**: 867-875.